
ON EXPLORING PDE MODELING FOR POINT CLOUD VIDEO REPRESENTATION LEARNING

Zhuoxu Huang¹ Zhenkun Fan¹ Tao Xu³ Jungong Han^{1,2} ✉

¹Aberystwyth University ²University of Sheffield

³Shanghai Investigation Design and Research Institute Co., Ltd.

zhh6@aber.ac.uk

✉ corresponding author jungonghan77@gmail.com

ABSTRACT

Point cloud video representation learning is challenging due to complex structures and unordered spatial arrangement. Traditional methods struggle with frame-to-frame correlations and point-wise correspondence tracking. Recently, partial differential equations (PDE) have provided a new perspective in uniformly solving spatial-temporal data information within certain constraints. While tracking tangible point correspondence remains challenging, we propose to formalize point cloud video representation learning as a PDE-solving problem. Inspired by fluid analysis, where PDEs are used to solve the deformation of spatial shape over time, we employ PDE to solve the variations of spatial points affected by temporal information. By modeling spatial-temporal correlations, we aim to regularize spatial variations with temporal features, thereby enhancing representation learning in point cloud videos. We introduce Motion PointNet composed of a PointNet-like encoder and a PDE-solving module. Initially, we construct a lightweight yet effective encoder to model an initial state of the spatial variations. Subsequently, we develop our PDE-solving module in a parameterized latent space, tailored to address the spatio-temporal correlations inherent in point cloud video. The process of solving PDE is guided and refined by a contrastive learning structure, which is pivotal in reshaping the feature distribution, thereby optimizing the feature representation within point cloud video data. Remarkably, our Motion PointNet achieves an impressive accuracy of 97.52% on the MSRAction-3D dataset, surpassing the current state-of-the-art in all aspects while consuming minimal resources (only 0.72M parameters and 0.82G FLOPs).

1 Introduction

Point cloud video modeling has emerged as a forefront topic in fields such as autonomous driving and robotics, primarily due to its ability to represent the variations in our 3D real world. A core problem in point cloud video modeling lies in efficient spatial-temporal representation learning (Song et al., 2022) from the intricate point cloud video data.

Unlike the continuous grid structure in traditional video data, point cloud videos are challenging to process. This is due to the point cloud video combining the unordered structure in spatial space and the ordered structure in temporal space. The uncertainty of correlation between frames hampers the application of explicit motion field capture in point cloud video learning. Without explicitly solving the point-wise correspondence, some standard models have been designed to extract dynamic information for point cloud video modeling. For instance, some methods adopt two-stream structures (Zhong et al., 2022; Liu and Xu, 2021; Liu et al., 2022) to decouple the spatial and temporal information for separate processing. Additionally, a popular model family (Fan et al., 2021b, 2022, 2021a, 2023) employs both the spatial convolution and the temporal convolution with a sophisticated designed 4D convolution to directly process the point cloud video. Several fusion strategies (Liu and Xu, 2021; Liu et al., 2022) and transformer-based post-process module (Fan et al., 2021a, 2023) have been adopted after the process of spatial and temporal dimensions separately. However, the absence of motion field solving brings defects to these methods, where the spatial irregularity negatively impacts the temporal modeling, and vice versa. Our observation demonstrates that this drawback constrains the alignment and uniformity (see Figure 1) of feature distributions. Such alignment and uniformity have been demonstrated to exert

beneficial effects on downstream tasks (Wang and Isola, 2020), especially for video learning (Pu et al., 2022). The mere fusion of disparate spatial and temporal features cannot effectively mitigate this issue, emphasizing the pressing need for a more effective method of learning point cloud video representations. We provide more details in the following Section 2.

In this paper, we aim to improve the representation of point cloud video learning by effectively modeling the spatial-temporal correlations in point cloud video to enhance alignment and uniformity. To this end, we leverage partial differential equations (PDE), widely used in physical modeling, to formulate point cloud video representation learning as solvable PDEs. We demonstrate its effectiveness as an optimal method for spatio-temporal modeling within the point cloud video domain.

Our idea is inspired by the analogy between fluid systems in the physical domain and point cloud video representations. Firstly, both systems aim to study the deformation of spatial points over time due to motion, conceptualized as a unified representation across spatial and temporal dimensions. This representation is akin to the velocity field in fluid systems and the motion field in point cloud videos. PDEs are widely used as a powerful modeling tool to describe such phenomena involving changes in spatial and temporal dimensions (Tran et al., 2021; Liu et al., 2023). Secondly, PDE models applied to such physical systems are typically employed in discretized, high-dimensional coordinate spaces (*i.e.* point cloud coordinate) to ensure solvability (Wu et al., 2023a). These considerations make the application of PDEs in the point cloud video domain particularly intuitive.

Our Motion PointNet is a pioneering approach that applies PDE-solving to point cloud video data. Specifically, we adopt PDE to model the spatial-temporal correlations and regularize the spatial variations with temporal features. It consists of two main components: Firstly, a **PointNet-like encoder** is adopted for the initial state of the spatial variations of points. Instead of processing the spatial and temporal dimensions separately, we adopted the set abstraction (Qi et al., 2017) on the adjacent point cloud frames to generate local variations between frames. Secondly, we design our **PDE-solving module** to function as a cross-dimension (from temporal to spatial) feature reconstruction process from the masked token. The idea is to represent how spatial information is affected by temporal variations. We design a contrastive learning structure for this PDE-solving process. Our PDE-solving module functions by supervising the backbone through the backward propagation of the contrastive loss. This harmonizes the dichotomy between the comparative learning task and the downstream task (Khosla et al., 2020).

We conduct extensive experiments to demonstrate the significant advancements achieved by our Motion PointNet in the study of point cloud video. Our Motion PointNet improves the performance of the point cloud video action recognition task by a clear margin. Extensive experiments on various benchmarks including MSRAAction-3D (Li et al., 2010), NTU RGB+D (Shahroudy et al., 2016), and UTD-MHAD (Chen et al., 2015) prove the superiority of our proposal. Prominently, with only 0.72M parameters and 0.82G FLOPs, our Motion PointNet achieves an accuracy of 97.52% on the MSRAAction-3D dataset. Furthermore, by leveraging the unsupervised contrastive learning mechanism, we explore the self-supervised potential of the PDE-solving module, offering pre-trained models for further investigation.

In summary, the contributions of this work can be outlined as follows:

- We propose a brand-new perspective that views the process of point cloud video representation learning as a PDE-solving problem. The novelty lies in the reconstruction of spatial information from the temporal dimension as the PDE-solving target. By doing so, we can establish a synthesis of unified representation across spatial spaces and temporal spaces, thereby enhancing the point cloud video representation learning.
- We design a lightweight PointNet-like encoder and a PDE-solving module to capture the spatial-temporal correlations in the point cloud video. These components form the foundation of our Motion PointNet framework, tailored for the task of point cloud video understanding.

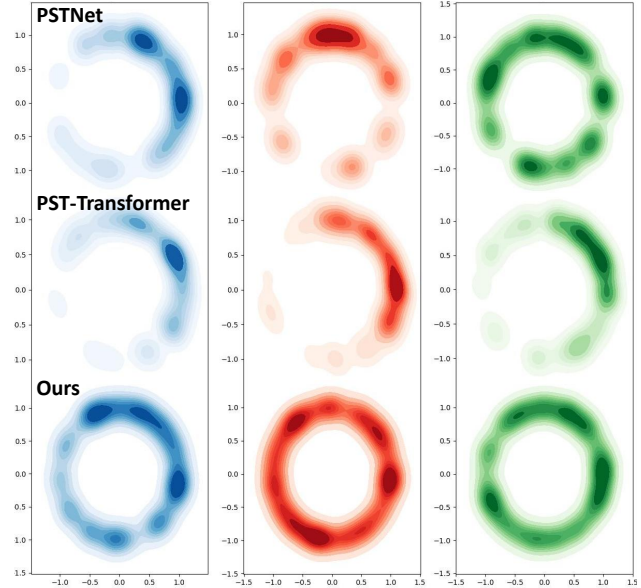


Figure 1: Representations of MSRAAction-3D test set on hypersphere. The temporal uniformity, spatial uniformity, and final logits uniformity are present in blue, red, and green, respectively. Feature vectors should ideally be uniformly distributed over a unit hypersphere. The uniformity demonstrates the integrity of the information in features.

2 Priori Observations

To our knowledge, we are the first to adopt PDE models in the point cloud video domain. In this section, we explore the motivation behind this idea and verify the interpretability of point cloud video feature representation. We conduct proof-of-concept validation to reveal the intrinsic relationship between spatio-temporal representations and model performance.

2.1 Preliminary

While we require both spatial and temporal information to well present the point cloud video data, the lack of explicit motion field capturing in the current models could bring drawbacks in feature representation. Due to the inherent complexity of the spatial-temporal structure of point cloud video data, the mutual negative impacts between spatial and temporal modeling are inevitable (Fan et al., 2023). We quantify such drawbacks in the representation with the spatial-temporal alignment loss and the uniformity loss:

$$\mathcal{L}_{\text{align}} \triangleq \left(\frac{1}{N} \sum_{i=1}^N \|x_i^S - x_i^T\|_2^\alpha \right), \text{ and } \mathcal{L}_{\text{uniform}} \triangleq \log \left(\frac{1}{\binom{N}{2}} \sum_{i < j} e^{-t\|x_i - x_j\|_2^2} \right), \quad (1)$$

where the N represents the sample number of the validation data, x represents a feature representation of a data sample, and superscript S and T stand for ‘spatial’ and ‘temporal’, respectively.

The alignment loss quantifies the discrepancy between a data sample’s spatial and temporal dimensions. Ideally, both the spatial and temporal features can obtain the same logit distribution. Such alignment ensures consistent distribution between the spatial and temporal representation. Meanwhile, the uniformity loss indicates the thoroughness of the representation (Wang and Isola, 2020). Ideally, feature vectors should be uniformly distributed over a unit hypersphere to maintain the integrity of the information. We set $\alpha = 2$ and $t = 2$ following the standard setting in Wang and Isola (2020).

2.2 Alignment and Uniformity of Spatial-Temporal Representations

We evaluate the alignment and uniformity of the representation from previous state-of-the-art models, PSTNet (Fan et al., 2021b) and PST-Transformer (Fan et al., 2023), and compare them with our proposed method. The spatial and temporal representations are decomposed from the last-layer backbone feature, utilizing a pooling operation along the corresponding dimension. We perform the alignment loss and the uniformity loss in Table 1 and Figure 1, and show their effect on model performance.

PSTNet adopts a 4D convolution for point cloud video data, where the spatial and temporal information are separately abstracted from different convolutions. It maintains the uniformity of the representations to a certain extent. However, the performance of the model is hindered by the negative effects arising from processing the dimensions separately. To mitigate this issue, PST-Transformer adopts a transformer module after the 4D convolution layers. Although merging spatial and temporal features reduces the spatial-temporal alignment loss to some extent, it also disrupts the uniformity of the overall feature representations. Unlike others, our Motion PointNet preserves feature uniformity and enhances the alignment of spatial and temporal representations, thereby significantly boosting model performance. By adopting PDE-solving for unified spatio-temporal representation, our model outperforms the previous state-of-the-art to a great extent.

Table 1: Alignment loss and uniformity loss of spatial-temporal representations from MSRAAction-3D test set.

	alignment(↓) S-T	T	uniformity(↓) S	logit	Acc.(%)(↑)
PSTNet (Fan et al., 2021b)	1.1421	-1.2254	-1.2501	-1.5494	91.20
PST-Transformer (Fan et al., 2023)	<u>0.3937</u>	-1.1260	-1.0573	-1.1614	<u>93.73</u>
Ours	0.0368	-1.5305	-1.5718	-1.5642	97.52

3 Related Works

3.1 Point Cloud Video Understanding

Point cloud video contains complex spatial-temporal information and combines an intricate structure with both unordered (intra-frame) and ordered (inter-frame) nature. Early methods either simplify its structure by dimensionality reduction using projections (Luo et al., 2018), or adopt voxelization to construct a regulated grid-based data (Choy et al., 2019; Wang et al., 2020). Similar to projections/voxel-based methods in static point clouds, those methods also faced information loss and issues with processing efficiency. Recent methods (Liu et al., 2019; Min et al., 2020; Fan et al., 2021b,a) inclined to process the point cloud video directly with set abstraction (Qi et al., 2017). For instance, Fan et al. (2021b) proposed a 4D convolution that implicitly captures the dynamic of adjacent point cloud frames by adopting the set abstraction between them and processes the point cloud sequence recursively. After that, an improved version (Fan et al., 2022) proposed to enhance dynamic capture with an additional temporal convolution. These point-based methods focus more on the motion representation and try to improve the dynamic capture process in different aspects. P4Transformer (Fan et al., 2021a) and PST-Transformer (Fan et al., 2023) captured dynamic by searching related points in the spatial-temporal space with attention-based networks. Kinet (Zhong et al., 2022) proposed a kinematics-inspired neural network and solved the dynamic capture in point cloud sequence using scene flow. Our Motion PointNet is built upon a brand-new perspective that treats the process of representation learning in point cloud video as a solvable PDE problem.

3.2 PDE-Solving with Deep Models

Our work is also related to solving PDE numerically with deep models. The PDE-solving problem has been widely explored with spectral methods since the last century (Gottlieb and Orszag, 1977; Fornberg, 1998). Recently, some research work explored the deep models for PDE due to their great nonlinear modeling capability (Li et al., 2020; Tran et al., 2021; Fanaskov and Oseledets, 2022; Liu et al., 2023). Additionally, PDE has garnered interest in vision research, finding applications in tasks like point cloud compression (Yang et al., 2023) and video prediction (Wu et al., 2023b). In this study, we endeavor to implement PDE in point cloud video understanding tasks. To this end, we have developed a novel Motion PointNet model utilizing PDE for the spatial-temporal correlations in point cloud video, thereby enhancing motion representation and raising performance in these tasks. To the best of our knowledge, this is the first application of PDE in this domain.

4 Proposed Method

We illustrate the proposed Motion PointNet for point cloud video in detail in the following sections. Figure 2 shows the overall architecture of the Motion PointNet, which is composed of a PointNet-like encoder and a PDE-solving module.

4.1 PointNet-like Encoder

We design a lightweight yet effective encoder for the initial spatial variations in our Motion PointNet. Given a point cloud with N points that presented as $P = \{p_1, p_2, \dots, p_N\}$, where each point $p_i \in \mathbb{R}^3$ is specified by the geometric coordinates $\{x, y, z\}$. A point cloud video contains T frames of point clouds presented as $V = \{P_1, P_2, \dots, P_T\}$, combining characteristics of both unordered intra-frame and ordered inter-frame. Previous methods (Fan et al., 2021b,a, 2023) process the point cloud video V recursively by sophisticated designed 4D convolutions. Differently, we process T frames of data as batches following previous video networks (Lin et al., 2019; Wang et al., 2019), thus processing the point cloud video with the shape of $\{B \times T, N, C\}$. Here a ‘batch’ represents a group of data entered into the network for training, and the ‘batch size’ represents the number of training samples in each batch. Here the *batch size* = $B \times T$. Usually, $C = 3$ represents the spatial coordinates $\{x, y, z\}$.

We then extend the spatial encoder from PointNet++ (Qi et al., 2017) for static point clouds only to the temporal domain. For a static point cloud P , Qi et al. (2017) adopt a multilayer perceptron (MLP) for spatial set abstraction:

$$Feature = f(P, P'), \quad (2)$$

where f represents a standard PointNet++ layer. We omit some basic operations in point cloud processing to simplify the description (e.g. sampling and grouping for the generation of P' from P). Here P functions as the support points and P' is the downsampled query points from the original P . We recommend referring to PointNet++ (Qi et al., 2017) for more details. Equation (2) can be extended and further formed as follows when using batch processing, thus easily fitting our reshaped point cloud video:

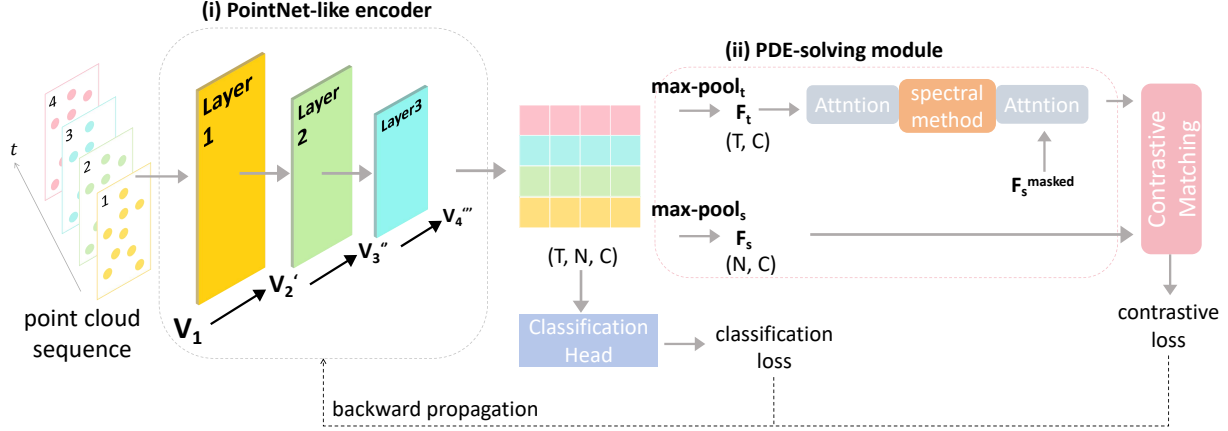


Figure 2: Overall architecture of our Motion PointNet. **PointNet-like Encoder:** Benefiting from the rolling operation, as the network goes deeper, features from the current frame are continually aggregated to the next frame, while also perceiving more spatial information with a larger spatial receptive field. **PDE-solving module:** We then further refine the motion information by formulating this process as solvable PDE. The PDE-solving module provides additional supervision of the backbone with a cross-dimension feature reconstruction target.

$$Feature = f(\{P_1, P_2, \dots\}, \{P_1, P_2, \dots\}') = f(V, V'). \quad (3)$$

However, the simple spatial encoder still lacks temporal consciousness and cannot well present the motion information. We solve this problem by adding a *rolling* operation *i.e.* `torch.roll()` on the temporal dimension which leads to frame misalignment in point cloud videos. In other words, we generate the support points and the query points from different point cloud frames instead of the same one to aggregate ‘motion’ from $P_t \rightarrow P_{t+1}$:

$$Feature = f(P_t, P'_{t+1}). \quad (4)$$

Here, the P_t functions as the support points and P'_{t+1} is the downsampled query points from the next point cloud frame P_{t+1} . When using batch processing, Equation (4) can be reformulated as follows:

$$Feature = f(\{P_1, P_2, \dots, P_t, \dots\}, \{P_2, P_3, \dots, P_{t+1}, \dots\}') = f(V_1, V_2'), \quad (5)$$

where the index of V represents the temporal index of the first point cloud frame in the point cloud sequence. In this way, the spatial set abstraction is extended to the temporal domain by operating on the adjacent frames while keeping its lightness and simplicity. We naturally stack multiple PointNet++ layers to build our PointNet-like encoder. As the network delves deeper, simultaneous temporal rolling and spatial abstraction persist, resulting in the expansion of the encoder’s receptive fields in both spatial and temporal dimensions. Taking a 3-layer depth encoder as an example:

$$Layer_1 = f(V_1, V_2') \quad Layer_2 = f(V_2', V_3'') \quad Layer_3 = f(V_3'', V_4'''), \quad (6)$$

where more superscript ‘ represents the larger spatial sampling scale than the previous layer. Different from previous methods, our encoder maintains the sequence length T while aggregating temporal information from the current frame to the next frame, greatly enhancing the local information density of our features.

4.2 PDE-solving Module

Building temporal-to-spatial mapping. Given the spatial-temporal feature acquired from the encoder $Feature \in \mathbb{R}^{T \times M}$, where $M < N$ is the number of spatial regions after aggregation. Subsequently, we proceed with max-pooling in both the temporal and spatial dimensions, respectively, and obtain the sub-global temporal feature $F_t \in \mathbb{R}^T$ and the sub-global spatial feature $F_s \in \mathbb{R}^M$. We target reconstructing the F_s from a learnable parameters set F_s^{masked} by reversing the F_t with spectral methods (see Figure 3 (b)). Both the F_t and the F_s are in the Banach spaces $\mathcal{F} = \mathcal{F}(\mathcal{D}; \mathbb{R}^{d_F})$, where $\mathcal{D} \subset \mathbb{R}^d$ is a bounded open set. Based on assumptions from Lu et al. (2021) and Li et al. (2021b), we can solve the PDE with a deep model \mathcal{M}_θ by approximating the optimal operator. This process can be formulated as follows:

$$\mathcal{M} : F_t \xrightarrow{\theta} F_s, \quad (7)$$

where θ is the learnable parameter set. Our PDE-solving module directly incorporates the feature variations over time as the variable θ in the modeling process. This allows the PDE to capture a more accurate and nuanced representation of how point cloud features evolve compared to previous temporal modeling approaches. Our approach also differs from the existing reconstruction-based method that mainly addresses the inner data distribution patterns by reconstructing masked tokens (see Figure 3 (a)). These methods focus on either the spatial or temporal dimension solely and are usually sensitive to mask ratio. Furthermore, simply recovering the masked data does not meet our purposes of spatial-temporal correlation modeling.

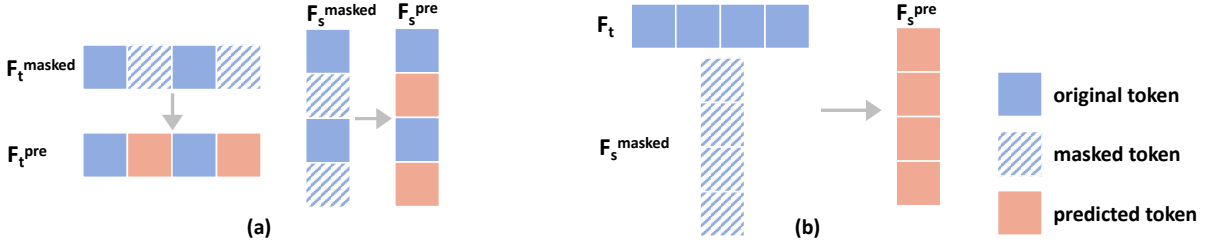


Figure 3: Comparison between reconstruction target for (a) inner data distribution and (b) spatial-temporal correlation modeling.

Solving PDE mapping. We then introduce the core of the PDE-solving module with a spectral method. The approximating of θ in Equation (7) can be formulated as follows:

$$\mathcal{M}_\theta = \sum_{i=1}^O w_i \mathcal{M}_{\theta,i}, \quad (8)$$

where O is the number of operators and w_i is learnable weight. As shown in Figure 2 (iii), the core of the PDE-solving module is composed of a multi-head self-attention (MHSA) layer, a spectral method layer, and a multi-head cross-attention (MHCA) layer. Although a simplistic deep model (Liu et al., 2023) can be used for PDE-solving, the design attempts to learn the operator as a whole ($O = 1$) while still maintaining network efficiency is challenging due to the complexities of input-output mappings in high-dimensional space (Wu et al., 2023a; Karniadakis et al., 2021). We tackle this problem with the combination of the attention mechanism and the classic spectral method (Tolstov, 2012) for PDE, which decomposes complex nonlinear mappings into multiple basis operators, while also holding the universal approximation capacity with theoretical guarantees.

For every $\mathbf{f}_t \in F_t$, we use trigonometric as the basis operators following Lu et al. (2021) and Li et al. (2021b):

$$\mathcal{M}_{\theta,(2k-1)}(\mathbf{f}_t) = \sin(k\mathbf{f}_t), \quad \mathcal{M}_{\theta,(2k)}(\mathbf{f}_t) = \cos(k\mathbf{f}_t), \quad k \in \{1, \dots, N/2\} \quad (9)$$

where N is even. Then, the calculation of the mapping output can be formulated as follows:

$$F_{t \rightarrow s} = F_t + w_{\sin} [\mathcal{M}_{\theta,(2k-1)}(\mathbf{F}_t)]_{k=1}^{O/2} + w_{\cos} [\mathcal{M}_{\theta,(2k)}(\mathbf{F}_t)]_{k=1}^{O/2}. \quad (10)$$

Building upon the spectral method we elaborate above, we use a standard MHSA (Vaswani et al., 2017) layer to enhance the temporal feature before feeding into the spectral method layer. Furthermore, we align the two different Banach spaces of the mapping output $F_{t \rightarrow s}$ and F_s^{masked} by an MHCA layer and output the predicted \hat{F}_s .¹ The F_s^{masked} is initialized with the same shape as F_s .

Contrastive Matching Loss. We compare the predicted \hat{F}_s with the ground truth F_s using a contrastive-based InfoNCE loss (Oord et al., 2018) to refine the modeling of the spatial-temporal correlations to a distinct objective. We consider both the input F_t and the output F_s to contain more abstract information about the spatio-temporal features. By treating the \mathbf{f}_- in $Feature \in \mathbb{R}^{T \times M}$ before applying spatial/temporal pooling as the negative sample, we force the model to learn the implicit mapping between the spatial and temporal space, instead of reconstructing the de-pooling

¹We detail this process in Appendix A

feature by closer both F_t and F_s to *Feature* (which is against the learning objectives). For every $\hat{\mathbf{f}}_s \in \hat{F}_s$, we treat the corresponding token in F_s as positive sample \mathbf{f}_{s+} . The loss function can be formulated as follows:

$$\mathcal{L} = \sum_{\hat{\mathbf{f}}_{s,i} \in \hat{F}_s} -\log \frac{\exp(\hat{\mathbf{f}}_{s,i}^T \mathbf{f}_{s+} / \tau)}{\exp(\hat{\mathbf{f}}_{s,i}^T \mathbf{f}_{s+} / \tau) + \sum_{\mathbf{f}_{-,j} \in \text{Feature}} \exp(\hat{\mathbf{f}}_{s,i}^T \mathbf{f}_{-,j} / \tau)}, \quad (11)$$

where τ is a temperature that controls the network sensitivity to positive and negative samples. Several ablation studies in Section 5.3 underscore the superiority of our loss design.

5 Experiment

5.1 Experimental Settings

We evaluate the proposed Motion PointNet on three benchmarks including the MSRAction-3D (Li et al., 2010) dataset, NTU RGB+D (Shahroudy et al., 2016) dataset and UTD-MHAD (Chen et al., 2015) dataset for point cloud video action recognition. We conduct all our experiments on the NVIDIA A100 GPUs. Following the previous works (Zhong et al., 2022; Fan et al., 2021b, 2023; Chen et al., 2015), we use default data splits in all evaluated datasets for fair comparisons.

Training Settings. We evaluate our Motion PointNet using several training strategies including end-to-end training, pre-train and fine-tuning, and linear probing. Leveraging the contrastive learning mechanism, we found that pre-train and fine-tuning can bring the most improvement in Section 5.3 and report them as our main results in the following sections. We pre-train our Motion PointNet with the PDE-solving module and only fine-tune the encoder we proposed in Section 4.1 with a classification head. We report results from the fine-tuned models. We further investigate the self-supervised potential of the PDE-solving module on other backbone models.

Table 2: Comparison with current state-of-the-art on MSRAction-3D dataset.

Methods	Accuracy(%) of different frame rate				
	4-frame	8-frame	12-frame	16-frame	24-frame
MeteorNet (Liu et al., 2019)	78.11	81.14	86.53	88.21	88.50
P4Transformer (Fan et al., 2021a)	80.13	83.17	87.54	89.56	90.94
PSTNet (Fan et al., 2021b)	81.14	83.50	87.88	89.90	91.20
SequentialPointNet (Li et al., 2021a)	77.66	86.45	88.64	89.56	91.94
PointMapNet (Li et al., 2023)	79.04	84.93	87.13	89.71	91.91
PSTNet++ (Fan et al., 2022)	81.53	83.50	88.15	90.24	92.68
Kinet (Zhong et al., 2022)	79.80	83.84	88.53	91.92	93.27
3DInAction (Ben-Shabat et al., 2023)	80.47	86.20	88.22	90.57	92.23
PST-Transformer (Fan et al., 2023)	81.14	83.97	88.15	91.98	93.73
Motion PointNet	79.46	85.88	90.57	93.33	97.52

5.2 Action Recognition Results

MSRAction-3D dataset includes 567 depth map sequences of 20 action classes performed by 10 subjects. To generate point cloud videos from the original data, we adopt the standard method following Liu et al. (2019) and Fan et al. (2021b,a), and report the average accuracy of our experiment over 10 runs following the convention. We compare our Motion PointNet to prior works in Table 2. Our report proves that the proposed method outperforms the current SOTA by significant margins, gaining a **+3.79%** accuracy with 24-frame input. Furthermore, it maintains superior performance with reduced frame input (12/16-frame), demonstrating the robustness of the proposed Motion PointNet. The performance on 4/8-frame MSRAction-3D indicates a slight limitation on short video input with a comparable accuracy. Indicate that the simple and explicit temporal informativeness of adjacent frames is proportional to the length of the input video.

Notably, the proposed method not only attains state-of-the-art performance but also surpasses existing models in terms of model parameters, complexity, and running time. As illustrated in Table 3, previous approaches that rely on sophisticated 4D convolutions are usually accompanied by intricate computational demands and substantial learning

Table 3: Qualitative results for efficiency evaluation on MSRAction-3D. Notice that the reported runtime results are on 24-frame MSRAction-3D.

Methods	flames	FLOPs(G)	Param.(M)	Acc.(%)	time(ms)
PSTNet (Fan et al., 2021b)		54.09	8.44	89.90	63.88
MeteorNet (Liu et al., 2019)		1.70	17.60	88.21	80.11
P4Transformer (Fan et al., 2021a)	16	40.38	42.07	89.56	25.18
PST-Transformer (Fan et al., 2023)		-	44.20	91.98	69.37
Kinet (Zhong et al., 2022)		10.35	3.20	91.92	-
Motion PointNet	16/24	0.55/0.82	0.72	93.33/ 97.52	1.17

parameters. For instance, PSTNet (Fan et al., 2021b) is composed of a hierarchical architecture with 4-layer 4D convolutions, which result in over 50G FLOPs. When further improving the performance by even more complex networks (Fan et al., 2021a, 2023), the learning parameters reach a staggering 40M+. Differently, our Motion PointNet miniaturizes the model in both FLOPs and learning parameters to the SOTA level. Remarkably, our Motion PointNet surpasses the current state-of-the-art with a **0.55G** FLOPs (when comparing at a 16-frame input) and **0.72M** learning parameters. We further visualize the points corresponding to high feature response in Appendix B, please check for details.

NTU RGB+D dataset contains 60 action classes and 56,880 video samples, which is a large-scale dataset consisting of complex scenes with noisy background points. We report the results of the cross-subject and cross-view scenarios following the official data partition (Shahroudy et al., 2016). We compare our Motion PointNet to prior works in Table 4. Our report proves that the proposed method maintains its superiority on the large-scale dataset. Our Motion PointNet is superior to most of the methods with different input modalities including depth map, skeleton, and dense points. It consistently outperforms the large model including PSTNet (Fan et al., 2021b), P4Transformer (Fan et al., 2021a), and PST-Transformer (Fan et al., 2023) in both the cross-subject (92.9% accuracy) and cross-view (98.0% accuracy) protocols, while forming a way more lightweight network. As shown in Table 5, our Motion PointNet offers consistent superiority in lightweight regarding model parameters (1.64M parameters) and computational complexity (15.47G FLOPs).

Table 4: Compare to the current state-of-the-art on NTU RGB+D dataset.

Methods	Modalities	Cross Subject	Cross View
Li et al. (Li et al., 2018)		68.1	83.4
Wang et al. (Wang et al., 2018)	depth map	87.1	84.2
MVDI (Xiao et al., 2019)		84.6	87.3
SkeleMotion (Caetano et al., 2019)		69.6	80.1
DGNN (Shi et al., 2019)	skeleton	89.9	96.1
MS-G3D (Liu et al., 2020)		91.5	96.2
3DV (Wang et al., 2020)		88.8	96.3
P4Transformer (Fan et al., 2021a)		90.2	96.4
PST-Transformer (Fan et al., 2023)		91.0	96.4
Kinet (Zhong et al., 2022)	points	92.3	96.4
PSTNet (Fan et al., 2021b)		90.5	96.5
PSTNet++ (Fan et al., 2022)		91.4	96.7
PointMapNet (Li et al., 2023)		89.4	96.7
SequentialPointNet (Li et al., 2021a)		90.3	97.6
Motion PointNet	points	92.9	98.0

Table 5: Qualitative results for efficiency evaluation on NTU RGB+D dataset.

Model	FLOPs(G)	PARAMS(M)
PSTNet (Fan et al., 2021b)	19.58	8.52
PointMapNet (Li et al., 2023)	-	2.65
P4Transformer (Fan et al., 2021a)	48.63	65.17
PST-Transformer (Fan et al., 2023)	48.68	65.19
GeometryMotion-Net (Liu and Xu, 2021)	68.42	40.44
Motion PointNet	15.47	1.64

We also report the hyper-settings of our Motion PointNet for the two aforementioned datasets in Table 6. We modified the basis hyperparameters in the table and selected the best-setting group in our experiments. The NTU RGB+D dataset

Table 6: Hyper-settings of our Motion PointNet.

	Dataset	MSRAAction-3D	NTU RGB+D
Encoder Setting	Input points \times frames	2048 \times 24	2048 \times 24
	Number of encoder layers	3	5
	Spatial stride	32, 8, 2	8, 8, 1, 1, 4
	K-neighbors	48, 32, 8	32, 48, 16, 24, 32
	Output feature channel	1024	1024
PARAMS(M)	w/o PDE-solving	0.72	1.64
	w/ PDE-solving	5.95	6.83
FLOPs(G)	w/o PDE-solving	0.82	15.47
	w/ PDE-solving	1.06	15.73

requires a deeper network due to its complex scenes and large scale. Notice that our PDE-solving module is also lightweight with only additional +5.2M parameters and +0.2G FLOPs in both settings.

Table 7: Compare to the current state-of-the-art on UTD-MHAD benchmark.

Methods	Accuracy(%)
SequentialPointNet (Li et al., 2021a)	92.31
PointMapNet (Li et al., 2023)	91.61
Motion PointNet	92.79

UTD-MHAD dataset contains 27 classes and 861 data sequences for action recognition. We apply our Motion PointNet to the UTD-MHAD benchmark and compare the proposed approach with current SOTA methods. The encoder settings of the Motion PointNet are consistent with the settings for the NTU RGB+D benchmark. Results in Table 7 illustrate the accuracy of different approaches. Our Motion PointNet maintains its superior performance with the highest accuracy of 92.79%.

5.3 Ablation studies

Ablation on Training Settings. Our pre-train and fine-tuning training process is designed to first allow the network to learn a robust spatial-temporal representation under the guidance of our PDE-solving module, and then to refine this representation using the classification head in the fine-tuning stage. In this way, we can keep our encoder as lightweight as possible while still enforcing its strong learning ability of the spatial-temporal correlations of the point cloud video data. To further demonstrate the effectiveness of our proposed method, we conduct two baseline comparisons in Table 8. The experiments are conducted on the MSR-Action3D Dataset with 24 frames.

Table 8: Ablation of different training settings for the Motion PointNet. Experiments are conducted on the MSRAAction-3D benchmark with 24 frames.

Settings	Accuracy(%)
pretrain + finetune	97.52
End-to-end	- 0.64
Linear probing	- 1.41

Here end-to-end training indicates training our Motion PointNet (encoder + PDE-solving module) with the classification head using the same number of iterations of the pre-train and fine-tuning training. Linear probing indicates fine-tuning the classification head while freezing the PointNet-like encoder to evaluate the pre-trained representation.

We also conduct extensive ablation experiments on the proposed Motion PointNet. Results in Table 9 show that the proposed encoder itself has outperformed the PST-Transformer (Fan et al., 2023) with a 95.76% accuracy. Furthermore, the PDE-solving module brings a significant improvement (+1.75% accuracy) to our encoder. We also implement our PDE-solving module on the PST-Transformer. After pertaining together with our PDE-solving module, the PST-Transformer encoder also achieved a +1.32% accuracy improvement. This underscores the universality of our PDE-solving module and the applicability of the PDE-solving perspective across different scenarios in point cloud video action recognition.

Table 9: Ablation on PDE-solving module. Experiments are conducted on the MSRAAction-3D benchmark.

Methods	Accuracy(%)
PST-Transformer (Fan et al., 2023)	93.73
+ PDE-solving	95.05 (+1.32)
Our Encoder	95.76
+ PDE-solving	97.52 (+1.76)

We further validate the effectiveness of different components in the PDE-solving module. Results are shown in Table 10. Firstly, we assess the individual contributions of the three layers that constitute the core of PDE-solving module. We observe that the spectral method primarily contributes to the performance enhancement, with the MHSA and MHCA layers also demonstrating their indispensability. The following results prove the utility of our contrastive matching loss. Other measures including cosine similarity and L2 distance are not ideal when we want to maximize the similarity between representations since they are either insensitive to linear scale or unbounded and harder to optimize. Finally, we validate different reconstruction targets in the PDE-solving module. The performance decays when we attempt to model inversely by solving $F_s \rightarrow F_t$ instead of $F_t \rightarrow F_s$. We hypothesize that this phenomenon arises because F_t preserves a higher degree of integrated temporal information and the PDE is more explanatory with the $F_t \rightarrow F_s$ target.

Table 10: Ablation of different components of PDE-solving module. Experiments are conducted on the MSRAction-3D benchmark.

Settings		Accuracy(%)
full PDE-solving module		97.52
PDE-solving core	w/o MHSA	- 0.71
	w/o spectral method	- 1.14
	w/o MHCA	- 0.41
w/o contrastive matching	L2 similarity	- 0.63
	Cosine similarity	- 0.43
w/ contrastive matching	InfoNCE loss	± 0 .
reconstruction targets	$F_s \rightarrow F_t$	- 0.68
	$F_t \rightarrow F_s$	± 0 .

6 Conclusion

We have presented a novel architecture called Motion PointNet for point cloud video representation learning through PDE-solving. Our approach leverages a lightweight PointNet-like encoder and a specialized PDE-solving module to establish a unified spatio-temporal representation, enhancing point cloud video learning significantly. Our extensive experiments across multiple benchmarks demonstrate the superiority of Motion PointNet, achieving state-of-the-art accuracy with notably reduced model complexity. This work not only advances the field of point cloud video representation learning but also opens new avenues for future research on efficient and effective motion capture in point clouds. The remarkable results underscore the potential of PDE-based solutions in addressing complex spatio-temporal data challenges. In future work, we aim to further extend our Motion PointNet to an extensive range of point cloud video understanding tasks including segmentation, detection, and object tracking.

References

- Ben-Shabat, Y., Shrout, O., and Gould, S. (2023). 3dinaction: Understanding human actions in 3d point clouds. *arXiv preprint arXiv:2303.06346*.
- Caetano, C., Sena, J., Brémond, F., Dos Santos, J. A., and Schwartz, W. R. (2019). Skelemotion: A new representation of skeleton joint sequences based on motion information for 3d action recognition. In *2019 16th IEEE international conference on advanced video and signal based surveillance (AVSS)*, pages 1–8. IEEE.
- Chen, C., Jafari, R., and Kehtarnavaz, N. (2015). Utd-mhad: A multimodal dataset for human action recognition utilizing a depth camera and a wearable inertial sensor. In *2015 IEEE International Conference on Image Processing (ICIP)*, pages 168–172.
- Choy, C., Gwak, J., and Savarese, S. (2019). 4d spatio-temporal convnets: Minkowski convolutional neural networks. In *Proceedings of the IEEE/CVF Conference on Computer Vision and Pattern Recognition*, pages 3075–3084.
- Fan, H., Yang, Y., and Kankanhalli, M. (2021a). Point 4d transformer networks for spatio-temporal modeling in point cloud videos. In *IEEE/CVF Conference on Computer Vision and Pattern Recognition, CVPR*.
- Fan, H., Yang, Y., and Kankanhalli, M. (2023). Point spatio-temporal transformer networks for point cloud video modeling. *IEEE Transactions on Pattern Analysis and Machine Intelligence*, 45(2):2181–2192.

- Fan, H., Yu, X., Ding, Y., Yang, Y., and Kankanhalli, M. (2021b). Pstnet: Point spatio-temporal convolution on point cloud sequences. In *International Conference on Learning Representations*.
- Fan, H., Yu, X., Yang, Y., and Kankanhalli, M. (2022). Deep hierarchical representation of point cloud videos via spatio-temporal decomposition. *IEEE Transactions on Pattern Analysis and Machine Intelligence*, 44(12):9918–9930.
- Fanaskov, V. and Oseledets, I. (2022). Spectral neural operators. *arXiv preprint arXiv:2205.10573*.
- Fornberg, B. (1998). *A practical guide to pseudospectral methods*. Number 1. Cambridge university press.
- Gottlieb, D. and Orszag, S. A. (1977). *Numerical analysis of spectral methods: theory and applications*. SIAM.
- Karniadakis, G. E., Kevrekidis, I. G., Lu, L., Perdikaris, P., Wang, S., and Yang, L. (2021). Physics-informed machine learning. *Nature Reviews Physics*, 3(6):422–440.
- Khosla, P., Teterwak, P., Wang, C., Sarna, A., Tian, Y., Isola, P., Maschinot, A., Liu, C., and Krishnan, D. (2020). Supervised contrastive learning. *Advances in neural information processing systems*, 33:18661–18673.
- Li, J., Wong, Y., Zhao, Q., and Kankanhalli, M. S. (2018). Unsupervised learning of view-invariant action representations. *Advances in neural information processing systems*, 31.
- Li, W., Zhang, Z., and Liu, Z. (2010). Action recognition based on a bag of 3d points. In *2010 IEEE Computer Society Conference on Computer Vision and Pattern Recognition - Workshops*, pages 9–14.
- Li, X., Huang, Q., Wang, Z., Hou, Z., and Yang, T. (2021a). Sequentialpointnet: A strong parallelized point cloud sequence network for 3d action recognition. *arXiv preprint arXiv:2111.08492*.
- Li, X., Huang, Q., Zhang, Y., Yang, T., and Wang, Z. (2023). Pointmapnet: Point cloud feature map network for 3d human action recognition. *Symmetry*, 15(2).
- Li, Z., Kovachki, N., Azizzadenesheli, K., Liu, B., Bhattacharya, K., Stuart, A., and Anandkumar, A. (2020). Fourier neural operator for parametric partial differential equations. *arXiv preprint arXiv:2010.08895*.
- Li, Z., Kovachki, N. B., Azizzadenesheli, K., liu, B., Bhattacharya, K., Stuart, A., and Anandkumar, A. (2021b). Fourier neural operator for parametric partial differential equations. In *International Conference on Learning Representations*.
- Lin, J., Gan, C., and Han, S. (2019). Tsm: Temporal shift module for efficient video understanding. In *Proceedings of the IEEE/CVF international conference on computer vision*, pages 7083–7093.
- Liu, J., Guo, J., and Xu, D. (2022). Geometrymotion-transformer: An end-to-end framework for 3d action recognition. *IEEE Transactions on Multimedia*, pages 1–13.
- Liu, J. and Xu, D. (2021). Geometrymotion-net: A strong two-stream baseline for 3d action recognition. *IEEE Transactions on Circuits and Systems for Video Technology*, 31(12):4711–4721.
- Liu, X., Xu, B., and Zhang, L. (2023). HT-net: Hierarchical transformer based operator learning model for multiscale PDEs.
- Liu, X., Yan, M., and Bohg, J. (2019). Meteornet: Deep learning on dynamic 3d point cloud sequences. In *ICCV*.
- Liu, Z., Zhang, H., Chen, Z., Wang, Z., and Ouyang, W. (2020). Disentangling and unifying graph convolutions for skeleton-based action recognition. In *Proceedings of the IEEE/CVF conference on computer vision and pattern recognition*, pages 143–152.
- Lu, L., Jin, P., Pang, G., Zhang, Z., and Karniadakis, G. E. (2021). Learning nonlinear operators via deeponet based on the universal approximation theorem of operators. *Nature machine intelligence*, 3(3):218–229.
- Luo, W., Yang, B., and Urtasun, R. (2018). Fast and furious: Real time end-to-end 3d detection, tracking and motion forecasting with a single convolutional net. In *Proceedings of the IEEE conference on Computer Vision and Pattern Recognition*, pages 3569–3577.
- Min, Y., Zhang, Y., Chai, X., and Chen, X. (2020). An efficient pointlstm for point clouds based gesture recognition. In *Proceedings of the IEEE/CVF Conference on Computer Vision and Pattern Recognition (CVPR)*.

- Oord, A. v. d., Li, Y., and Vinyals, O. (2018). Representation learning with contrastive predictive coding. *arXiv preprint arXiv:1807.03748*.
- Pu, S., Zhao, K., and Zheng, M. (2022). Alignment-uniformity aware representation learning for zero-shot video classification. In *2022 IEEE/CVF Conference on Computer Vision and Pattern Recognition (CVPR)*, pages 19936–19945.
- Qi, C. R., Yi, L., Su, H., and Guibas, L. J. (2017). Pointnet++: Deep hierarchical feature learning on point sets in a metric space. *Advances in neural information processing systems*, 30.
- Shahroudy, A., Liu, J., Ng, T.-T., and Wang, G. (2016). Ntu rgb+ d: A large scale dataset for 3d human activity analysis. In *Proceedings of the IEEE conference on computer vision and pattern recognition*, pages 1010–1019.
- Shi, L., Zhang, Y., Cheng, J., and Lu, H. (2019). Skeleton-based action recognition with directed graph neural networks. In *2019 IEEE/CVF Conference on Computer Vision and Pattern Recognition (CVPR)*, pages 7904–7913.
- Song, L., Gong, X., Planche, B., Zheng, M., Doermann, D., Yuan, J., Chen, T., and Wu, Z. (2022). Pref: Predictability regularized neural motion fields. In *European Conference on Computer Vision*, pages 664–681. Springer.
- Tolstov, G. P. (2012). *Fourier series*. Courier Corporation.
- Tran, A., Mathews, A., Xie, L., and Ong, C. S. (2021). Factorized fourier neural operators. *arXiv preprint arXiv:2111.13802*.
- Vaswani, A., Shazeer, N., Parmar, N., Uszkoreit, J., Jones, L., Gomez, A. N., Kaiser, Ł., and Polosukhin, I. (2017). Attention is all you need. In *Advances in neural information processing systems*, pages 5998–6008.
- Wang, P., Li, W., Gao, Z., Tang, C., and Ogunbona, P. O. (2018). Depth pooling based large-scale 3-d action recognition with convolutional neural networks. *IEEE Transactions on Multimedia*, 20(5):1051–1061.
- Wang, Q., Zhang, Y., Yuan, J., and Lu, Y. (2019). Space-time event clouds for gesture recognition: From rgb cameras to event cameras. In *2019 IEEE Winter Conference on Applications of Computer Vision (WACV)*, pages 1826–1835.
- Wang, T. and Isola, P. (2020). Understanding contrastive representation learning through alignment and uniformity on the hypersphere. In *International Conference on Machine Learning*, pages 9929–9939. PMLR.
- Wang, Y., Xiao, Y., Xiong, F., Jiang, W., Cao, Z., Zhou, J. T., and Yuan, J. (2020). 3dv: 3d dynamic voxel for action recognition in depth video. In *Proceedings of the IEEE/CVF conference on computer vision and pattern recognition*, pages 511–520.
- Wu, H., Hu, T., Luo, H., Wang, J., and Long, M. (2023a). Solving high-dimensional pdes with latent spectral models. In *International Conference on Machine Learning*.
- Wu, X., Lu, J., Yan, Z., and Zhang, G. (2023b). Disentangling stochastic pde dynamics for unsupervised video prediction. *IEEE Transactions on Neural Networks and Learning Systems*.
- Xiao, Y., Chen, J., Wang, Y., Cao, Z., Zhou, J. T., and Bai, X. (2019). Action recognition for depth video using multi-view dynamic images. *Information Sciences*, 480:287–304.
- Yang, X., Shao, Y., Liu, S., Li, T. H., and Li, G. (2023). Pde-based progressive prediction framework for attribute compression of 3d point clouds. In *Proceedings of the 31st ACM International Conference on Multimedia*, pages 9271–9281.
- Zhong, J.-X., Zhou, K., Hu, Q., Wang, B., Trigoni, N., and Markham, A. (2022). No pain, big gain: Classify dynamic point cloud sequences with static models by fitting feature-level space-time surfaces. In *Proceedings of the IEEE/CVF Conference on Computer Vision and Pattern Recognition (CVPR)*, pages 8510–8520.

A Details for the MHSA and MHCA layers

The MHSA layer and MHCA layer share the same structure but with different inputs. The MHSA layer uses the same F_t for query, key, and value generation. The MHCA layer uses the F_s^{masked} for query generation, and the mapping output $F_{t \rightarrow s}$ for key and value generation.

MHSA Firstly, the F_t is fed into a standard MHSA (Vaswani et al., 2017) module. We add the frame indexes as the position embedding. This process can be formulated as follows:

$$F_t = \text{PE}([1, 2, \dots, T]) + F_t, \quad (12)$$

$$H_m = \text{Softmax}(\{F_t W_m^Q\} \times \{F_t W_m^K\}^{Transpose} / \sqrt{d}) \times F_t W_m^V, \quad (13)$$

$$F_t = \text{Concat}(H_1, \dots, H_m), \quad (14)$$

where $\text{PE}(\cdot)$ is the positional encoding function that embeds the frame index to high-dimension. W_m^Q, W_m^K, W_m^V are learnable weights of the m th head for query, key, and value respectively. And d is the number of feature channels.

MHCA After getting the mapping output $F_{t \rightarrow s}$ from our spectral method layer, we align the two different Banach spaces of $F_{t \rightarrow s}$ and F_s by an MHCA layer. We execute this process with a learnable masked parameters set that is aligned with the F_s . This process can be formulated as follows:

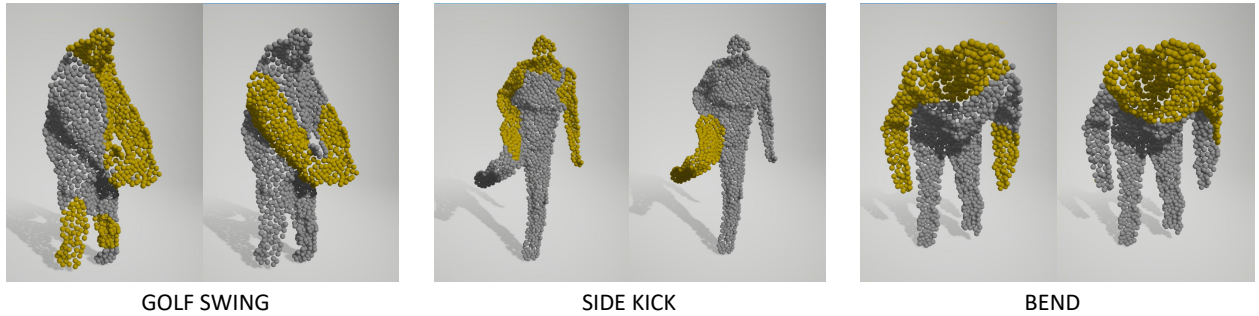
$$H_m = \text{Softmax}(\{F_s^{masked} W_m^Q\} \times \{F_{t \rightarrow s} W_m^K\}^{Transpose} / \sqrt{d}) \times F_{t \rightarrow s} W_m^V, \quad (15)$$

$$\hat{F}_s = \text{Concat}(H_1, \dots, H_m), \quad (16)$$

the F_s^{masked} is initialized with the same shape as F_s . We then match the predicted \hat{F}_s and the ground truth F_s as the supervision of the PDEs-solving.

B Visualization

We also report the feature response from PointNet++ (Qi et al., 2017) as further comparison with our Motion PointNet. The observation reveals that the PointNet++ model exhibits a response to regions where geometric features are distinctly pronounced, such as the head, shoulders, and arms, irrespective of whether these areas constitute the primary focus of the action. As we can see, in our Motion PointNet, the main moving part of actions (e.g. swinging arms in the golf swing) are highlighted, which is consistent with the proposed intuition.



Left: PointNet++ **Right:** Our Motion PointNet

Figure 4: Visualization comparison between PointNet++ and our Motion PointNet. High response points are marked in orange, which are selected based on the magnitude of the feature response. We choose binary representation for clarity in visualization.

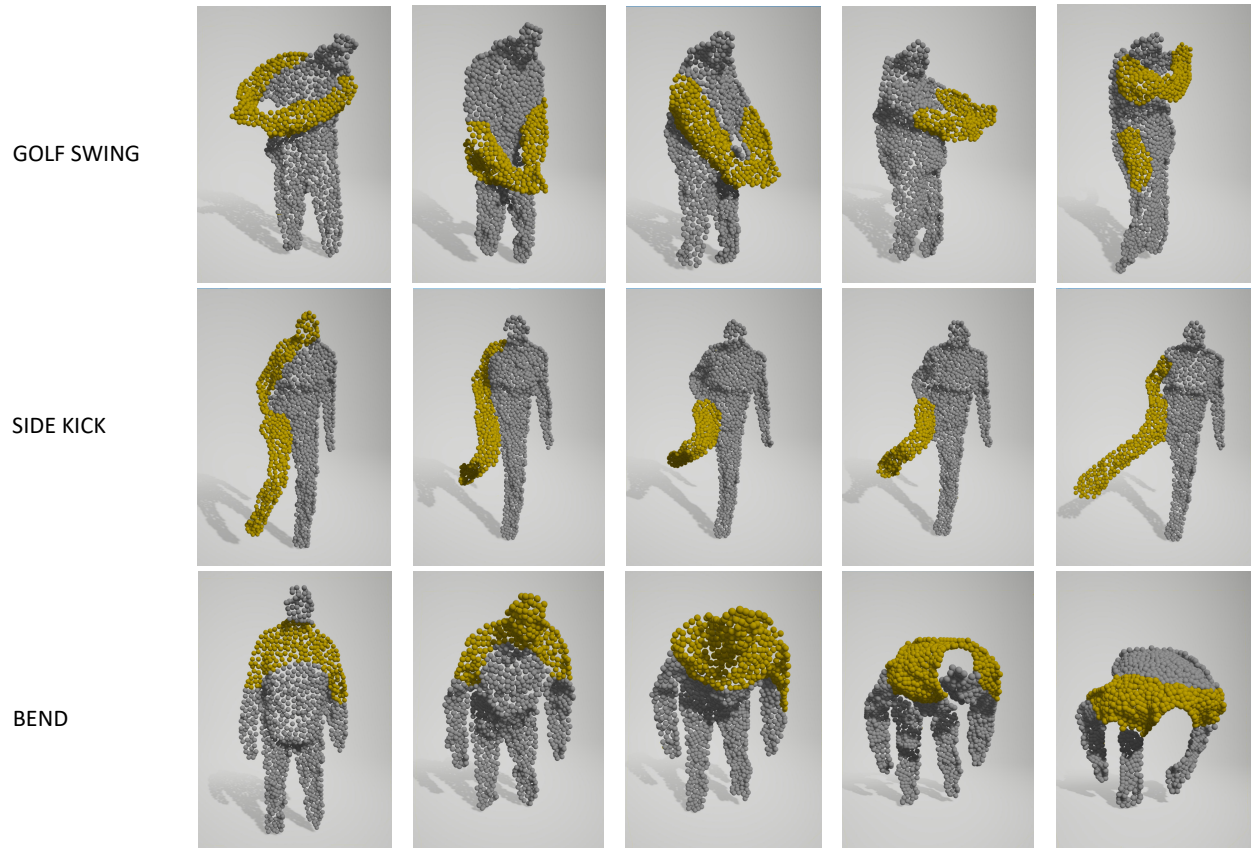


Figure 5: Visualization of high feature response on MSRAAction-3D dataset. High response points are marked in orange, which are selected based on the magnitude of the feature response. We choose binary representation for clarity in visualization.